Int. J. Heat Mass Transfer. Vol. 22, pp. 535–546

0017-9310/79/0401-0535 $02.00/0

FINITE AMPLITUDE BÉNARD–RAYLEIGH CONVECTION

J. R. KRASKA† and R. L. SANI‡

(*Received* 6 *March* 1978 *and in revised form* 14 *August* 1978)

Abstract—A nonlinear analysis of cellular convection driven by buoyancy and surface tension forces in a fluid layer of finite depth heated from beneath is described. The structure of slightly supercritical hexagonal and roll cell flow patterns and their associated heat flux is investigated. A stability analysis of possible flow states is described.

NOMENCLATURE

a_1, dimensionless coefficient;
$A_i(t)$, dimensionless amplitude;
b_i, dimensionless coefficients;
B, $= l^2 g\rho'/\sigma' (= Ra/Ma)$;
C_h, dimensionless third order solvability coefficient;
C_p, specific heat at constant pressure [J/kg K];
Cr, $= \kappa\mu/\sigma l$ (Crispation group);
$f(z)$, dimensionless Z-dependence of velocity;
$\mathscr{F}$, differential operator;
g, magnitude of acceleration of gravity [m/s^2];
G, $= \rho_0 g l^2(1+\zeta)/\sigma$ (gravity wave group);
h, heat-transfer coefficient at free surface [J/m^2 s K];
$\mathscr{H}$, dimensionless mean curvature;
H, dimensionless heat flux;
k, thermal conductivity [J/m s K];
$\mathbf{k}$, unit vector antiparallel to gravitational field;
l, layer depth [m];
$\mathscr{M}$, differential operator;
Ma, $= l\sigma'\Delta T/\kappa\mu$ (Marangoni group);
$\mathbf{n}$, unit outward pointing normal;
$\mathscr{N}$, differential operator;
Nu, $= hl/k$ (Nusselt group);
p, dimensionless pressure;
Pr, $= \mu C_p/k$ (Prandtl group);
s_i, dimensionless coefficients;
Ra, $= l^3 g\rho'\Delta T/\kappa\mu$ (Rayleigh group);
ΔT, temperature difference across layer [K];
T, dimensionless temperature;
$\mathbf{u}$, dimensionless velocity;
$\mathbf{V}$, dimensionless solution vector;
(x, y, z), dimensionless position coordinates.

Greek symbols

α, magnitude of wave vector;
$\boldsymbol{\alpha}$, dimensionless wave vector;
β, dimensionless linear growth rate;
β_2, transition point from hexagons to rolls;
γ, $= \Delta T/l$ [K/m];
δ, dimensionless z-variation of vertical vorticity;
ζ, thermal coefficient of expansion [K^{-1}];
η, dimensionless surface deflection;
θ, angle;
κ, thermal diffusivity of fluid [m^2/s];
μ, viscosity [Pa s];
Φ, (x, y, t) dependence of disturbance;
ϕ, (x, y) dependence of disturbance;
Ω, domain occupied by fluid layer;
$\partial\Omega$, boundary of domain Ω.

Subscripts

b, bottom of layer;
h, hexagons;
0, reference state;
r, rolls;
ss, steady state;
t, top of layer;
s, interface quantity.

Superscripts

$+$, transpose;
$*$, critical value or adjoint;
$'$, z-derivative;
$\dot{}$, t-derivative;
$\bar{}$, time average.

Other symbols

∇, gradient operator;
$\nabla\cdot$, divergence operator;
∇^2, Laplacian operator.

Scale factors

time: l^2/κ [s];
velocity: κ/l [m/s];
temperature: $(T_t - T_b)$, $T_b > T_t$ [K];
pressure: $\kappa\mu/l^2$ [N/m^2];
length: l [m].

†Upjohn Company, Kalamazoo, MI 49001, U.S.A.
‡Dept. Chemical Engineering, University of Colorado and CIRES, University of Colorado/NOAA, Boulder, CO 80309, U.S.A.

INTRODUCTION

THE SPONTANEOUS generation of form and structure has provided the stimulus for the study of many seemingly diverse physical phenomena. One such example is the spontaneous generation of flow, and concomitantly form, in an initially quiescent, horizontal layer of fluid in mechanostatic, but not thermostatic (or speciestatic) equilibrium. In many instances, the latter system exhibits a striking array of convection cells called after Bénard which are spatially periodic; in other cases very bizarre patterns are induced. The pioneering quantitative experimental results for thin fluid layers heated from below with the upper surface exposed to the atmosphere reported by Bénard stimulated Lord Rayleigh to propose and theoretically analyze a buoyancy driven prototype system. It is now well-known that the qualitative agreement between Rayleigh's theory and Bénard's experimental results was fortuitous since the cellular convection observed by Bénard was primarily surface tension driven. However, Rayleigh's analysis of the buoyancy driven prototype system provided impetus for not only linear stability theory in fluid mechanics, but also many subsequent investigations of Bénard convection. In fact, a recent survey of the literature by Velardé [1] lists more than 400 contributions; consequently, here in the interest of brevity the interested reader is referred to Chandrasekhar [2], Segel [3], Koschmieder [4] and Rogers [5] for comprehensive surveys.

The first investigation directly related to the surface tension aspects of the present work was due to Pearson [6] who proposed and analyzed the initiation of convection in a transversely infinite thin layer of fluid resting on a rigid surface heated from beneath. The flow was driven entirely by a surface tension gradient resulting from temperature variations along the free interface, that is, by a "surface engine". Scriven and Sternling [7], Smith [8], Berg and Acrivos [9] and Berg [10] refined Pearson's model by incorporating a more realistic interface. On the other hand Nield [12] combined the Rayleigh and Pearson models to analyze the initiation of convection driven by the combined surface tension–buoyancy mechanism and subsequently, he extended this analysis (Nield [12]). Nield's analyses established, as expected, the additivity of the two mechanisms in the generation of kinetic energy and also the dominance of the surface tension mechanism as the layer depth decreases. Some unusual experiments by Grodzka and Bannister [13] done during the flight of the Apollo XIV spaceship at 10^{-6} g demonstrated that surface tension gradients can lead to cellular convective motion when a certain critical temperature difference is exceeded but appeared to cast some doubt on the additivity of the two mechanisms. (A doubt not supported by linear theory or the nonlinear theory presented herein.)

The theoretical investigations cited previously are linear stability analyses which can predict a so-called critical temperature gradient at which a flow presumably first ensues and also the wave number, that is, a measure of the mean transverse cellular dimension, of the fastest growing disturbance. The deficiencies of the linear theory are the inability to predict the evolution of a disturbance and the final size and shape of the cellular structure. The intent here is to gain some additional insight into the combined surface tension–buoyancy mechanism by investigating the nonlinear stability problem. In particular, such nonlinear aspects as subcritical instabilities, convective heat flux and the prediction of stable spatial tessellations, such as rolls and hexagons, are considered. However, for simplicity the above properties are divorced from the question of cell size which is presumed to be known.

PROTOTYPE SYSTEM AND LINEAR STABILITY ANALYSIS

The prototype system to be investigated herein is a quiescent, thin, horizontal layer of Newtonian fluid of infinite horizontal extent resting on a heated, rigid surface of high thermal conductivity and capacity. Initially, a time-independent temperature field T_{ss} with a gradient of magnitude γ is present. That is,

$$T_{ss} = T_b + \gamma z. \tag{1}$$

The standard Boussinesq approximation (Spiegel and Veronis [14], Mihaljan [15]) is enforced with linear temperature variation of density in the buoyancy force term and of surface tension in the surface force term. The rigid bottom surface is likened to a metallic flat plate of very large thermal conductivity and capacity and consequently it is assumed that the velocity field vanishes and the temperature remains constant on the plate. The free surface is assumed to be deformable and in only thermal communication with the gas above it. Moreover, for simplicity the free surface is assumed to be Newtonian and is not endowed with surface shear or dilatational viscosities although these could easily be incorporated into the analysis.

The dimensionless mathematical characterization of the dynamics of the system can be cast in the following form:

$$\nabla^2 \mathbf{u} - \nabla p + BMa\mathbf{k}T = Pr^{-1}\left(\frac{\partial \mathbf{u}}{\partial t} + \mathbf{u}\cdot\nabla\mathbf{u}\right), \tag{2}$$

$$\nabla\cdot\mathbf{u} = 0, \tag{3}$$

$$\nabla^2 T - \mathbf{k}\cdot\mathbf{u} = \frac{\partial T}{\partial t} + \mathbf{u}\cdot\nabla T, \tag{4}$$

$$\mathbf{u} = 0,\ T = 0; \quad z = 0, \quad \text{all} \quad x, y, \tag{5}$$

$$\left.\begin{aligned}
&\mathbf{n}\cdot\nabla T + NuT = 0\\
&w - \frac{\partial\eta}{\partial t} - \mathbf{u}\cdot\nabla\eta = 0,\\
&2\mathbf{nn}:\nabla\mathbf{u} - p - Ma\mathbf{n}\cdot\nabla_s T - 2C_r^{-1}\mathscr{H} = 0,\\
&\nabla_s\cdot[\mathbf{n}\cdot\nabla\mathbf{u} + \mathbf{n}\cdot(\nabla\mathbf{u})^+] - \nabla_s\cdot(\mathbf{n}p) - 2C_r^{-1}\nabla_s\cdot(\mathbf{n}H) - Ma\nabla_s^2 T = 0,
\end{aligned}\right\} \quad z = 1+\eta(x,y) \text{ all } x,y \tag{6}$$

$$\mathbf{u},\quad T \sim \text{bounded}. \tag{7}$$

Here $\mathbf{u}$ is the velocity field, T the temperature field, p the pressure field and $\eta(x,y)$ characterizes the deviation of the free surface from its initial static position $z = 1$.

Most previous investigations known to the authors, except one due to Scanlon and Segel [16] which will be compared with the present study, deal with the linear stability problem. The linear stability problem and its companion adjoint problem which will be defined here play a fundamental role in the nonlinear analysis. Since the linear problem has been considered in detail elsewhere [17] only some of its more important aspects are recapped here.

LINEAR STABILITY ANALYSIS

The linear stability problem is generated by neglecting the nonlinear terms in equations (2)–(7) and linearizing boundary conditions (6) about $z = 1$ and the solution can be cast in the following general form [2]:

$$\mathbf{u}^{(1)} = \left\{ f_1(z)\Phi(x,y,t)\mathbf{k} + \frac{1}{\alpha^2}[Df_1\nabla_2\Phi - \delta_1(z)(\mathbf{k}x\nabla_2\Phi)] \right\} \tag{8}$$

$$T^{(1)} = g_1(z)\Phi(x,y,t).$$

Here $f(z)$, $\delta(z)$ and $g(z)$ are, respectively, the z-dependence of the vertical component of velocity and vorticity and the temperature, and $\Phi(x,y,t)$, called the planform function, is required to satisfy a two dimensional Helmholtz equation,

$$\nabla_2^2\Phi = -\alpha^2\Phi, \tag{9}$$

in which α, the wave number, is real-valued and according to linear theory

$$\dot{\Phi} = \beta\Phi.$$

The requirement that Φ be periodic in the horizontal plane leads to an infinitude of possible Φ's for a given value of α^2 as well as an infinite number (actually a continuum) of values of α^2. Since the present investigation is not concerned with the prediction of the lateral size of the convection cells, only Φ's of a given value of α^2 are of interest at this point. It should also be pointed out that $\delta_1 \equiv 0$ in equation (8) for the case being considered.

The substitution of expression (8) into the linearized version of equations (2)–(7) leads to an eigenvalue problem which was solved numerically by using a fourth order Runge–Kutta scheme as an alternative to evaluation of the exact solution because it afforded a better foundation on which to build the subsequent calculations required by the nonlinear theory. (The accuracy of the scheme was checked by comparison with exact solutions.) Marginally stable solutions to the linear stability problem were generated over a wide range of parameter space. It is noteworthy in this respect that the results of Scriven and Sternling [7] indicate that if the Crispation number exceeds approximately 10^{-3} there exist no nontrivial values of the Marangoni number corresponding to a marginal stability state. However, as pointed out by Smith [8] the inclusion of gravity waves at the interface in bi-layered systems remedies the problem in many cases. The gravity wave contribution was included in the present analysis but here also instances were encountered in which the Marangoni number exhibited either no minimum or only a relative minimum as a function of wave number (see Table 1). In this regard it is noteworthy that the inclusion of gravity wave effects results in the appearance of a gravity wave number, G, which appears only in the free surface boundary conditions. Its primary effect is on the magnitude of the surface deflection whose maximum is

$$b = \frac{Crh(1)}{\alpha^2\left(\dfrac{G}{\alpha^2}+1\right)}, \tag{10}$$

where $h(1)$ is a function of the vertical velocity, Cr is the Crispation number and α is the wave number. The basic effect of G on the stability of the system is to shift the critical wave numbers to smaller values, that is, to produce larger cells at onset. This effect is easily detectable by a perusal of Tables 1 and 2 which also illustrate the occurrence of critical Marangoni numbers for some cases in which Crispation number is 10^{-2}. The occurrence of downflow under depressions in the tessellated surface for a primarily buoyancy driven flow and the reverse for primarily surface tension driven flows is predicted by the linear theory and substantiated by observation (see Table 2).

Typical variations of critical Marangoni number and corresponding wave number as displayed in Fig. 1 and detailed in Tables 1 and 2. The minimum in critical wave number apparent in Fig. 1 occurs in all cases except the $Nu = 0$ cases and the case of $Cr = 10^{-3}$, $Nu = 0.5$ and reflects an interplay between the buoyancy and surface tension forces.

NONLINEAR ANALYSIS

If attention is restricted to disturbances and cellular flows of a single wave number, α, the

Table 1

Cr \ B	0	2	10	50	100	200	500	∞ ‡
				$Nu = 0.0, G = 0.0$				
	79.607†	65.081	37.086	11.571	6.2078	3.2204	1.3176	669.00
0	1.993	1.994	2.016	2.058	2.070	2.078	2.082	2.086
	79.496	65.092	37.140	11.580	6.2105	3.2210	1.3177	669.00
10^{-4}	1.988	1.993	2.018	2.060	2.071	2.078	2.082	2.086
	78.476	65.192	37.639	11.661	6.2353	3.2279	1.3187	669.00
10^{-3}	1.947	1.983	2.036	2.072	2.079	2.082	2.084	2.086
				$Nu = 0.5, G = 0.0$				
	98.256	78.587	42.807	12.813	6.8156	3.1592	1.4356	727.42
0	2.142	2.136	2.151	2.188	2.199	2.205	2.209	2.212
	98.151	78.611	42.855	12.816	6.8151	3.5182	1.4351	727.07
10^{-4}	2.139	2.134	2.152	2.188	2.198	2.204	2.208	2.210
	97.182	78.835	43.299	12.843	6.8098	3.5092	1.4299	723.89
10^{-3}	2.106	2.129	2.164	2.187	2.192	2.194	2.195	2.196
				$Nu = 2.0, G = 0.0$				
	150.68	113.39	55.202	15.148	7.9285	4.0584	1.6467	831.27
0	2.386	2.357	2.353	2.378	2.384	2.388	2.391	2.393
	150.57	113.44	55.234	15.140	7.9226	4.0548	1.6451	830.40
10^{-4}	2.384	2.356	2.353	2.376	2.382	2.386	2.388	2.390
	149.57	113.94	55.523	15.072	7.8685	4.0215	1.6303	822.44
10^{-3}	2.360	2.354	2.353	2.358	2.359	2.360	2.360	2.361

†Upper number is Ma^* and lower number is α^*.
‡Here the critical value of Rayleigh number and corresponding wave number are listed.

Table 2

G \ B	0	0.7	10	50	100	∞
			$Nu = 0.0, Cr = 0.01$			
			44.470(+)	12.568(+)	6.4991(+)	669.00(+)
0	‡	‡	2.296§	2.204	2.154	2.086
			44.102(+)	12.524(+)	6.4863(+)	669.00(+)
0.2	‡	‡	2.272§	2.193	2.147	2.086
	68.975(−)†	68.389(−)	42.865(+)	12.376(+)	6.4439(+)	669.00(+)
1	1.501§	1.663§	2.914	2.156	2.126	2.086
	78.799(−)	73.500(−)	37.501(+)	11.642(+)	6.2296(+)	669.00(+)
50	1.978	1.979	2.012	2.059	2.071	2.086
			$Nu = 0.5, Cr = 0.01$			
			49.428(+)	13.145(+)	6.7427(+)	688.41(+)
0	‡	‡	2.351§	2.175§	2.107§	2.012§
		84.697(−)	49.111(+)	13.130(+)	6.7466(+)	690.46(+)
0.2	‡	1.733§	2.331§	2.174	2.113	2.033
	88.359(−)	86.163(−)	48.050(+)	13.080(+)	6.7587(+)	696.57(+)
1	1.793	1.906	2.271	2.170	2.131	2.083
	97.373(−1)	90.085(−)	43.223(+)	12.839(+)	6.8106(+)	724.30(+)
50	2.128	2.126	2.146	2.184	2.194	2.206

†Upper number is Ma^* and lower number is α^*. (+) or (−) indicates upflow under, respectively, surface elevation or depression.
‡No minimum.
§Relative minimum.

nonlinear stability problem can be posed in the following manner: Given a disturbance whose (x, y, t) dependence Φ is

$$\Phi = \sum_{m=1}^{N} A_m(t)\phi_m(x, y), \tag{11}$$

$$\nabla_2^2 \phi_m = -\alpha^2 \phi_m, \tag{11a}$$

what are the possible stable equilibrium sets $\{A_m(\infty)\}$ and associated convective transport?

The particular form Φ is suggested by the general Fourier integral representation theorem and is employed because of one's inability to handle the integral representation. The mathematical tool used in analyzing the nonlinear stability problem is a

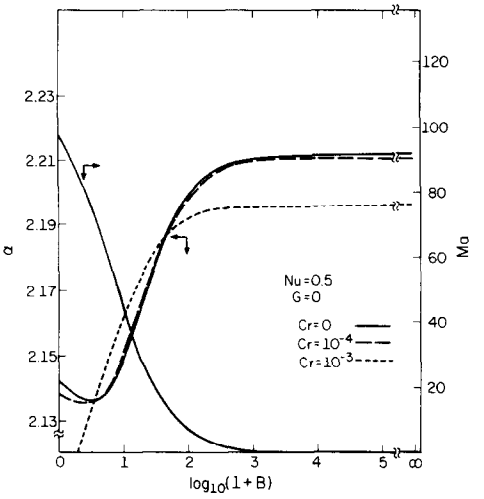

FIG. 1. Linear stability critical states.

modification of an asymptotic perturbation technique due to Stuart [18] and Watson [19]. (See Segel [3] for a discussion of the method and Segel and Stuart [20] and Sani [21] for particular applications.) By adding $-\beta Pr^{-1}\mathbf{u}$ and $-\beta T$ respectively to equations (2) and (4), a form of the nonlinear equations appropriate for the present analysis is generated. In addition if

$$\mathbf{V} \equiv \begin{pmatrix} u \\ v \\ w \\ T \end{pmatrix}, \tag{12}$$

then operators $\mathscr{M}$, $\mathscr{F}$ and $\mathscr{N}$ can be defined in an obvious fashion such that equations (2) and (4) can be rewritten in the following operator form:

$$\mathscr{M}(\mathbf{V}) - \beta\mathscr{F}(\mathbf{V}) = \mathscr{N}(\mathbf{V}). \tag{13}$$

The complete specification of the system is obtained by appending equations (3), (5), (6) and (7) to equation (12).

The fundamental building block for the nonlinear theory is the linear stability problem which here is cast in the form

$$\mathscr{M}(\mathbf{V}^{(1)}) - \beta\mathscr{F}(\mathbf{V}^{(1)}) = \mathbf{0}, \tag{14}$$

plus the continuity equation (3) and the boundary data (5), (6) and (7). For simplicity it is necessary to invoke the so-called principle of exchange of stabilities, that is, the property that β is real-valued. (The latter property has been verified by Vidal and Acrivos [22] and also by the present authors for a layer with no surface deflection, that is, $Cr = 0$; however, a cursory investigation of the general case does not preclude the possibility of overstability in general and especially if the ratio (Pr/Cr) is sufficiently small.) In this case the marginal linear stability problem corresponds to $\beta = 0$ and leads to a critical Marangoni number Ma^* and a critical wave number α^*. (The latter also corresponds to the fastest growing disturbance if $Ma > Ma^*$ that is $\beta > 0$.) The linear growth rate factor β corresponding to any value of Ma can be computed from the characteristic equation associated with the linear stability problem and for β close to zero is approximately proportional to $(Ma - Ma^*)$.

The exponential amplification of an unstable disturbance according to linear theory is completely unacceptable in the light of physical observations. Therefore, it might be expected that a perturbation scheme which starts with the entire space–time dependence of linear theory might encounter some difficulty—the erroneous conclusions of Struminskii [23] serve as a good example. However, it is experimentally observed that apparently the spatial dependence predicted by linear theory is a rather good approximation in many cases. (See Stuart [24] for a comprehensive discussion of this point.) Consequently, the starting point of the perturbation scheme outlined here is the linear theory solution, equation (8), coupled with the planform function Φ of equation (9) in which the set of amplitudes $\{A_m(t)\}$ are unspecified. That is,

$$\mathbf{u}^{(1)} = \sum_{m=1}^{N} A_m \left\{ f_1(z)\phi_m \mathbf{k} + \frac{1}{\chi^2}\left[Df_1 \nabla_2 \phi_m - \delta_1 (\mathbf{k} x \nabla_2 \phi_m) \right] \right\} \equiv \sum_{m=1}^{N} A_m \mathbf{u}_m^{(1)},$$

$$T^{(1)} = \sum_{m=1}^{N} A_m g_1 \phi_m \equiv \sum_{m=1}^{N} A_m T_{1m},$$

and accordingly,

$$\mathbf{V}^{(1)} = \begin{pmatrix} \mathbf{u}^{(1)} \\ T^{(1)} \end{pmatrix} = \sum_{m=1}^{N} A_m \mathbf{V}_m^{(1)}. \tag{15}$$

The basic step in the perturbation scheme is the determination of evolution equations for the amplitude set $\{A_m(t)\}$ at each step. Actually, only the asymptotic evolution for times which are large enough such that initial conditions have no effect are of interest. The perturbation scheme can be formulated in the following abstract manner:

$$\mathscr{M}(\mathbf{V}^{(n)}) - \beta\mathscr{F}(\mathbf{V}^{(n)}) = \mathscr{N}(\mathbf{V}^{(n-1)}), \quad n = 2,3,\ldots, \tag{16}$$

with $\mathbf{V}^{(1)}$ given by equation (15). Additionally, the continuity equation and boundary conditions must be satisfied by each $\mathbf{V}^{(n)}$. Here $\mathscr{N}(\mathbf{V}^{(n-1)})$ is the nonlinear operator $\mathscr{N}(\mathbf{V}^{(n-1)})$ truncated at terms of order n in the amplitudes $\{A_m(t)\}$. It is noteworthy that the present method neglects initial conditions. However, a similar technique can be used to solve the initial value problem, and the present results are good approximations outside of a "time boundary layer" near zero time, that is, a region in which the solution is strongly affected by the initial data. The two solutions agree exactly in the limit of infinite time.

At each stage of the perturbation scheme a nonhomogeneous boundary value problem must be

solved. In order for a solution to exist the "solvability condition",

$$\lim_{\beta \to 0} [\, \mathbf{f}^{(n)}(\mathbf{V}^{(n-1)}), \mathbf{V}_1^*] = 0, \quad n \geqslant 2. \tag{17}$$

must be satisfied for all time. Here

$$(\mathbf{A}, \mathbf{B}) \equiv \sum_{i=1}^{5} \int_{\Omega} A_i B_i \, d\Omega, \tag{18}$$

and $\mathbf{V}_1^*$ is the solution to the adjoint system:

$$\nabla^2 \mathbf{u}^* - P_r^{-1} \nabla^* p = 0, \tag{19}$$

$$\nabla \cdot \mathbf{u}^* = 0, \tag{20}$$

$$\nabla^2 T^* - \mathbf{k} \cdot \mathbf{u}^* = 0, \tag{21}$$

$$\mathbf{u}^* = \mathbf{0}, \quad T^* = 0 \quad \text{on} \quad z = 0, \tag{22}$$

$$\left.\begin{aligned} &\frac{\partial T^*}{\partial z} + NuT^* - Ma \nabla_2^2 \frac{\partial W^*}{\partial z}, \\ &W^* = 0, \\ &\nabla_2 \cdot \frac{\partial \mathbf{u}^*}{\partial z} + \nabla W^* = 0, \end{aligned}\right\} \text{ on } z = 1 \tag{23}$$

$$\mathbf{u}^*, \ T^* \text{ remain bounded.} \tag{24}$$

The solutions of the adjoint system may be written in a form similar to equation (8). The evolution equations for the amplitude set $\{A_m(t)\}$ are generated in fulfilling the solvability condition, equation (16).

AMPLITUDE EQUATIONS

The evolution equations for the amplitude set $\{A_m(t)\}$, hereafter referred to as amplitude equations, are generated by satisfying the solvability condition, equation (17). The well-known linear theory approximation to the amplitude equations is

$$\dot{A}_m = \beta A_m, \quad m = 1, 2, \ldots, N. \tag{25}$$

As previously pointed out this form is unacceptable since it predicts either exponential growth or decay. Therefore, the modification of the amplitude equations by the nonlinear theory is of prime concern. The form of the amplitude equation may be modified whenever the nonlinear operator $\mathbf{f}^{(n)}(\mathbf{V}^{(n-1)})$ generates a vector whose (x,y)-dependence is identical to one of the original $\mathbf{V}_m^{(1)}$ associated with equation (15). The latter is called (x,y)-replication after Segel [25]. (It should be pointed out that Segel's definition of replication also takes into account z-dependence of the vector.)

It has been established by Scanlon and Segel [16] and others that for (x,y)-replication to occur at second order it is required that the product of two planform functions, say ϕ_i and ϕ_j, of the initial set contains a term proportional to one of the initial planform functions, say ϕ_k. The process can best be visualized by using the exponential form of the solution to equation (11a) for then a set Ω of 2-D vectors can be associated with the set $\{\phi_j\}$. Then the replication property follows if $\boldsymbol{\alpha}_k = \boldsymbol{\alpha}_j$ with $\boldsymbol{\alpha}_k, \boldsymbol{\alpha}_i, \boldsymbol{\alpha}_j \in \Omega$; that is, the three wave vectors form an equilateral triangle. (Note that all the original planform functions $\{\phi_i, i = 1,2,\ldots,N\}$ have the same wave number and hence all associated wave vectors have the same length.) Similarly, at third order (x,y)-replication can only occur if the product of planform functions associated with the second order solution $\mathbf{V}^{(2)}$ and the initial planform functions contains a term proportional to one of the initial planform functions. In terms of wave vectors the third order replication process corresponds to formation of a general triangle.

According to linear theory a system is stable if $\beta < 0$; however, in certain systems a so-called subcritical instability can occur due to nonlinear effects – the present system is an example. (See, for example, Sani [21], Joseph and Shir [26], and Segel and Stuart [24] for discussions of subcritical instabilities.) If a subcritical instability is to be predicted, the amplitude equations of linear theory, equation (25), must be modified by the solvability requirement of the higher order perturbation equations. This modification is first possible at second order. In the latter case the first components $\mathbf{V}_m^{(1)}$ of the linear solution which have a possibility of growing for $\beta < 0$, that is, can modify their amplitude equations, are associated with those planform functions, or equivalently, wave vectors, which satisfy the second order replication property. Associated with each wave vector are two real planform functions, and it can be shown that there is a one parameter family of six planform functions, or associated $\mathbf{V}_m^{(1)}$'s, which have the first opportunity to lead to an instability. (See Segel [25] for a discussion of this point with respect to the buoyancy driven case.) The parameter associated with the family specifies the orientation of the tessellations. Consequently, if it is assumed that only one family starts growing the parameter can be chosen to be zero since the stability of the various tessellations in an infinite plane should be independent of their orientation. The restriction to the initial growth of only one family implies that systems with rather uniform cellular patterns are being studied.

When the second order terms in the amplitude equations of the most dangerous disturbances outweigh the stabilizing first order term for $\beta < 0$, their amplitudes grow. As the amplitudes become larger the third order terms in the amplitude equations are important. In the buoyancy driven case [25, 27], the third order terms in the amplitude equations of the first six disturbances to grow can be shown to be stabilizing, that is, make a negative contribution to $\dot{A}_m^2$, $m = 1,2,\ldots,6$; consequently, when the first unstable disturbances start growing the remaining disturbances are just stabilized by third order terms. Subsequently, it is shown here that all third order terms need not be stabilizing in the case of the general surface tension-buoyancy driven flow.

For simplicity the stability investigation is initiated by considering a family of six disturbances which can first replicate at second order, that is, six disturbances which can possibly grow at a subcritical

value of the Marangoni number,

$$\Phi = A_1(t)\sin\frac{3^{1/2}}{2}\alpha x\sin\tfrac{1}{2}\alpha y + A_2(t)\cos\frac{3^{1/2}}{2}\alpha x\sin\tfrac{1}{2}\alpha y$$
$$+A_3(t)\sin\alpha y + A_4(t)\sin\frac{3^{1/2}}{2}\alpha x\cos\frac{\alpha}{2}y + A_5(t)\cos\frac{3^{1/2}}{2}\alpha x\cos\frac{\alpha}{2}y + A_6(t)\cos\alpha y, \quad (26)$$

plus a seventh disturbance

$$A_7(t)\cos m\alpha x\cos n\alpha y, \quad m^2+n^2 = 1. \quad (27)$$

Here it is restricted that $\theta \equiv \tan^{-1}(n/m)$ is not equal to $\pm 30°$ or $90°$. This restriction on θ is necessary in order to focus on only one "60°-triplet" of wave-number vectors plus one additional wave-number vector. (It is noteworthy that the seventh disturbance corresponds to a "rectangular tessellation" which is possible according to linear theory but which is disallowed by Stuart [24] on physical grounds.) The amplitude equations to third order are:

$$\dot{A}_1 = \beta A_1 + a_1(A_1A_6 - A_3A_4) - A_1[b_1(A_1^2+A_2^2+A_4^2)+b_2A_5^2+b_3(A_3^2+A_6^2)+b_6A_7^2] - \tfrac{1}{2}b_4A_2A_4A_5, \quad (28)$$

$$\dot{A}_2 = \beta A_2 + a_1(A_2A_6 - A_3A_5) - A_2[b_1(A_1^2+A_2^2+A_5^2)+b_2A_4^2+b_3(A_3^2+A_6^2)+b_6A_7^2] - \tfrac{1}{2}b_4A_1A_4A_5, \quad (29)$$

$$\dot{A}_3 = \beta A_3 - \frac{a_1}{2}(A_5A_2 + A_4A_1) - A_3[\tfrac{1}{2}b_3(A_1^2+A_2^2+A_4^2+A_5^2)+\tfrac{1}{2}b_3A_5^2+b_5(A_6^2+A_3^2)+b_7A_7^2], \quad (30)$$

$$\dot{A}_4 = \beta A_4 - a_1(A_4A_6 + A_1A_3) - A_4[b_1(A_1^2+A_4^2+A_5^2)+b_2A_2^2+b_3(A_3^2+A_6^2)+b_6A_7^2] - \tfrac{1}{2}b_4A_1A_2A_5, \quad (31)$$

$$\dot{A}_5 = \beta A_5 - a_1(A_5A_6 + A_2A_3) - A_5[b_1(A_2^2+A_4^2+A_5^2)+b_2A_1^2+b_3(A_3^2+A_6^2)+b_6A_7^2] - \tfrac{1}{2}b_4A_1A_2A_4, \quad (32)$$

$$\dot{A}_6 = \beta A_6 - \frac{a_1}{4}(A_4^2+A_5^2-A_1^2-A_2^2) - A_6[\tfrac{1}{2}b_3(A_1^2+A_2^2+A_4^2+A_5^2)+b_5(A_6^2+A_3^2)+b_7A_7^2], \quad (33)$$

$$\dot{A}_7 = \beta A_7 - A_7[b_6(A_1^2+A_2^2+A_4^2+A_5^2)+2b_7(A_3^2+A_6^2)+b_8A_7^2] \cdot (b_2 = b_1 - \tfrac{1}{2}b_4,\ b_4 = b_3 - b_5). \quad (34)$$

Note that second order terms do not appear in the seventh amplitude equation because the seventh disturbance cannot satisfy the (x,y)-replication requirement by interacting with any of the other six disturbances. Inclusion of other disturbances which do not replicate with the first six disturbances or among themselves leads to amplitude equations of the same form as equation (34). For example, inclusion of

$$A_8(t)\cos m\alpha x\sin n\alpha y, \quad (35)$$

$$A_9(t)\sin m\alpha x\cos n\alpha y, \quad (36)$$

$$A_{10}(t)\sin m\alpha x\sin n\alpha y, \quad (37)$$

leads to $\dot{A}_8$, $\dot{A}_9$, and $\dot{A}_{10}$ equations which are similar to $\dot{A}_7$ in that no second order terms appear.

At this point it is illuminating to perform a rotation of coordinates in order to transform the amplitude equations (28)–(34) into the form (see also Segel [25]):

$$\dot{B}_1 = \beta B - a_1B_2B_3\cos(\theta_1+\theta_2+\theta_3) - B_1(s_5B_1^2+s_8B_2^2+s_8B_3^2+s_3B_4^2) \quad (38)$$

$$\dot{B}_2 = \beta B_2 - a_1B_1B_3\cos(\theta_1+\theta_2+\theta_3) - B_2(s_8B_1^2+s_5B_2^2+s_8B_3^2+s_2B_4^2) \quad (39)$$

$$\dot{B}_3 = \beta B_3 - a_1B_1B_2\cos(\theta_1+\theta_2+\theta_3) - B_3(s_8B_1^2+s_8B_2^2+s_5B_3^2+s_1B_4^2) \quad (40)$$

$$\dot{B}_4 = \beta B_4 - B_4(S_3B_1^2+s_2B_2^2+s_1B_3^2+s_5B_4^2) \quad (41)$$

$$B_1\dot{\theta}_1 = a_1B_1B_3\sin(\theta_1+\theta_2+\theta_3) \quad (42)$$

$$B_2\dot{\theta}_2 = a_1B_1B_3\sin(\theta_1+\theta_2+\theta_3) \quad (43)$$

$$B_3\dot{\theta}_3 = a_1B_1B_2\sin(\theta_1+\theta_2+\theta_3), \quad (44)$$

where

$B_1^2 = A_3^2+A_6^2$, $B_2^2+B_3^2 = \tfrac{1}{2}(A_1^2+A_2^2+A_4^2+A_5^2)$,

$B_2^2-B_3^2 = A_1A_5 - A_2A_4$, $B_4 = A_7$,

$\theta_1 = -\tan^{-1}(A_3/A_6)$,

$\theta_2 = \tan^{-1}[(A_2-A_4)/(A_1+A_5)]$,

$\theta_3 = \tan^{-1}[(A_2+A_4)/(A_5-A_1)]$,

$s_1 = \tfrac{1}{2}C_0 + \tfrac{1}{2}(C_p+C_q)$, $s_2 = \tfrac{1}{2}C_0+\tfrac{1}{2}(C_r+C_s)$

$s_3 = \tfrac{1}{2}C_0 + \tfrac{1}{2} + \tfrac{1}{2}(C_m+C_n) = 2b_7$,

$s_5 = \tfrac{1}{2}C_0+\tfrac{1}{4}C_4$, $s_8 = b_3 = \tfrac{1}{2}C_0+\tfrac{1}{2}(C_1+C_3)$,

$q = 4-p$, $s = 4-5$, $n = 4-m$,

$b_1 = \frac{1}{16}(4C_0-2C_1-2C_3+C_4)$, $b_2 = \dfrac{(3s_5-s_8)}{4}$

$b_4 = s_8 - s_5$.

The values of p, r and m depend on the form chosen for the disturbance which is not in the "most dangerous triad" and are a function of

$$\theta \equiv \tan^{-1}(\alpha_y/\alpha_x)$$

associated with the wave vector $\boldsymbol{\alpha}$ of this disturbance. The coefficients C_h are obtained by evaluating the third order solvability condition (equation (16) with $n=3$) with $\mathbf{V}^{(2)}$ replaced by $\mathbf{V}_h^{(2)}$, the $h\alpha^2$-wave

number component of the second order solution

$$\mathbf{V}^{(2)} = \sum_h \mathbf{V}_h^{(2)}.$$

Some typical values of the coefficients s_5 and s_8 are tabulated in Table 3, and some typical C_h coefficients are displayed in Figs. 2–4. Figure 4 displays the behavior exhibited by the infinite layer model treated by Scanlon and Segel [16]. (In the latter case an analytic expression was developed, and the numerical integration scheme utilized in all other cases yields identical values to within roundoff error.) The coefficients a_1, s_5 and s_8 are necessary in the determination and assessment of the "primary stability" of equilibrium states and the C_h coefficients are necessary in the determination of the "secondary stability" of the equilibrium states. (Herein primary and secondary stability refer to stability relative to the six first replicating disturbances and to disturbances outside this set, respectively.)

Table 3

B	Cr	a_1	s_5	s_8	β_1	β_2	β_3
			$Nu = 0.0$, $G = 0.0$, $Pr = 8$				
0		−0.5817	0.7526	1.022	−0.0302	3.501	11.76
0.7		−0.5429	0.7151	0.9690	−0.0278	3.268	10.96
10	0.0	−0.2786	0.5173	0.6833	−0.0103	1.457	4.837
100		−0.04648	0.4151	0.5223	−0.0004	0.0781	0.2543
∞		0.0	0.4010	0.4979	0.0	0.0	0.0
0		−0.5893	0.8226	1.148	−0.0278	2.691	9.137
0.7		−0.5358	0.7060	0.9729	−0.0271	2.846	9.615
10	10^{-3}	−0.3087	0.5311	0.6746	−0.0127	2.461	8.047
100		−0.2336	1.880	2.264	−0.0029	0.6964	2.231
∞		−0.3150	6.168	7.359	−0.0012	0.4314	1.377
			$Nu = 0.0$, $G = 0.2$, $Pr = 8$				
0		−0.6349	0.9527	1.329	−0.0279	2.710	9.202
0.7	10^{-3}	−0.5711	0.7990	1.100	−0.0272	2.885	9.739
100		−0.2045	1.656	2.000	−0.0018	0.5874	1.884
∞		−0.2217	3.854	4.610	−0.0009	0.3314	1.059
			$Nu = 0.5$, $G = 1.0$, $Pr = 0.025$				
0		−0.6801	1.985	3.125	−0.0141	0.7072	2.528
0.7	10^{-2}	−1.086	2.779	4.036	−0.0272	2.075	7.162
10		−0.1861	0.2009	0.2465	−0.0125	3.343	10.79

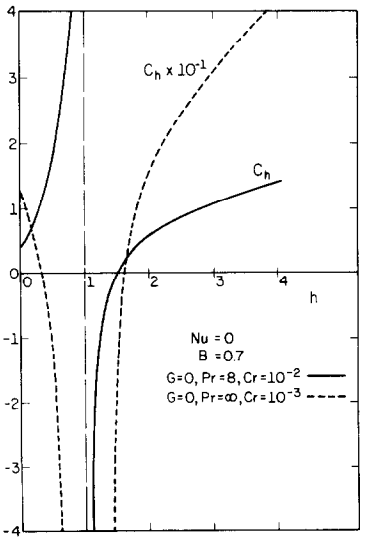

FIG. 2. Third order interaction coefficient for finite depth layer which is primarily surface tension driven.

EQUILIBRIUM STATES

There are five general types of equilibrium states associated with equations (38)–(44) (or equations (28)–(34)).

(1) *Hexagons*

$$B_{1e} = B_{2e} = B_{3e} = \frac{\pm[a_1 + (a_1^2 + 4\sigma S)^{1/2}]}{2S},$$
$$B_{4e} = B_{5e} = 0 \tag{45}$$
$$\sin(\theta_1 + \theta_2 + \theta_3) = 0, \quad S = 2s_8 + s_5,$$
$$\cos(\theta_1 + \theta_2 + \theta_3) = \pm 1.$$

(2) *Rolls*

$$B_{1e} = \pm(\sigma/s_5)^{1/2}, \quad B_{2e} = B_{3e} = B_{4e} = B_{5e} = 0. \tag{46}$$

(3) *Mixed-1*

$$B_{1e} = B_{5e} = \pm\left(\frac{\sigma}{s_5 + s_3}\right)^{1/2}, \quad B_{2e} = B_{3e} = B_{4e} = 0. \tag{47}$$

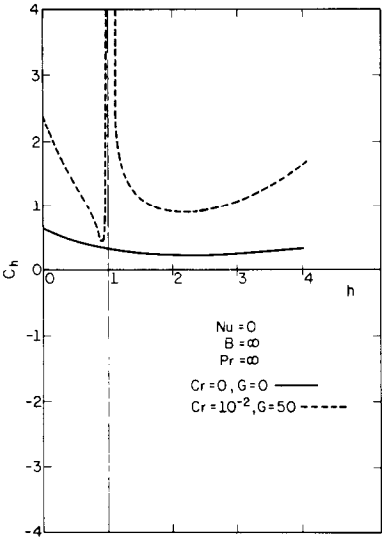

FIG. 3. Third order interaction coefficient for buoyancy driven finite depth layer.

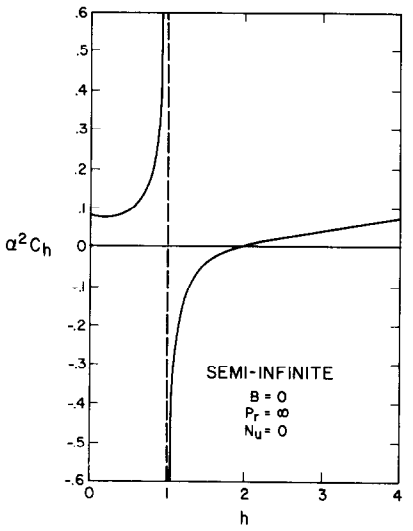

FIG. 4. Third order interaction coefficient for surface tension driven semi-infinite layer.

(4) *General polygons*

$$B_{2e} = B_{3e} = \pm\left[\frac{(\sigma - s_5\psi)}{(s_8+s_5)}\right]^{1/2}, \quad \psi \equiv \frac{a_1^2}{(s_8-s_5)}, \tag{48}$$

$$B_{1e} = \psi, \quad B_{4e} = B_{5e} = 0,$$
$$\sin(\theta_1+\theta_2+\theta_3) = 0,$$
$$\cos(\theta_1+\theta_2+\theta_3) = 1.$$

(5) *Mixed-2*

$$B_{1e} = B_{2e} = B_{3e} = 0,$$
$$B_{4e} = B_{5e} = \pm\left[\frac{\sigma}{(s_4+s_5)}\right]^{1/2}. \tag{49}$$

In all the cases considered herein s_5, s_8, s_8-s_5 are positive and consequently, the only possible subcritical equilibrium flow states are the hexagonal and the two mixed states and the latter require that s_5+s_3 and s_4+s_5 be negative.

STABILITY OF EQUILIBRIUM STATES

The stability of the equilibrium states was investigated by means of a linear stability analysis of the amplitude equations (38)–(44). This analysis established that in all cases investigated the general polygonal and the mixed states were unstable and hence only the hexagonal and roll equilibrium states need be considered. If initially attention is restricted to the six most dangerous modes (see equation (26)), the following constraints must be satisfied for asymptotic stability:

(a) *Hexagons*

$$\frac{-a_1^2}{4T} \leqslant \beta \leqslant \frac{a_1^2(s_8+2s_5)}{(s_8-s_5)^2}, \tag{50}$$

plus the restriction that if $a_1 < 0 (a_1 > 0)$, then the negative (positive) sign is selected within the brackets appearing in equation (45).

(b) *Rolls*

$$\beta \geqslant \frac{a_1^2 s_5}{(s_8-s_5)^2}. \tag{51}$$

Since the linear growth rate factor, β, is proportioned to $(Ma - Ma^*)$, stable hexagons can exist both subcritically and supercritically while stable rolls are restricted to supercritical states. This result is similar to that of Segel [3] for the thermoconvective case. Figure 5 illustrates this hierarchy of stable equilibrium states.

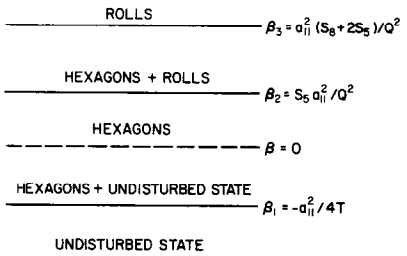

FIG. 5. Dynamic equilibrium states.

In the general case the additional disturbance leads to the following additional stability constraint:

(a) *Hexagons*

$$(s_1+s_2+s_3) \geqslant \beta/B_{6e}^2. \tag{52}$$

(b) *Rolls*

$$\beta(s_3-s_5)/s_5 \leqslant 0 \qquad (\beta \geqslant \beta_2). \tag{53}$$

Consequently if no disturbance can be found which violates these inequalities the hexagonal or roll solutions will also be stable to this disturbance; moreover, Segel [25] has shown that in this case the results of the seven disturbance analysis also are valid for the case of N-disturbances if one restricts attention to a single initial replicating triad and truncates at third order.

In the range of parameters investigated in this study rolls and hexagons were stable in all cases considered when attention was restricted to the six most dangerous modes, i.e. the first replicating triad in wave number space. Subcritical–supercritical hexagonal and supercritical roll solutions are stable for a finite depth, constant property (Boussinesq approximation) layer when both the surface tension and buoyancy mechanisms are active ($B \neq \infty$). The subcritical stability bound is well within the bound predicted by Davis [28] using an energy method. Also stable hexagonal solutions are possible for a buoyancy driven layer if the deflection of the free surface is taken into account; the latter is in accord with the analysis of Davis and Segel [29]. The width of the band of stable hexagonal solutions (constant wave number), $\beta_3 - \beta_1$, which is proportional to a ΔMa, or ΔRa, is an increasing function of Prandtl number, Pr, and Nusselt number, Nu, and attains a maximum as a function of the ratio of Rayleigh number to Marangoni number, B, if the Crispation number, Cr, is nonzero, i.e. the free surface is deformable and is a decreasing function of B if the free surface is non-deformable, $Cr = 0$.

The transition point from hexagonal solutions to roll solutions characterized by β_2 increases (decreases) as the width of the hexagonal band increases (decreases) and hence the occurrence of rolls becomes less (more) likely relative to hexagonal solutions.

The direction of flow in all cases (except for some anomalous behavior for small Prandtl number ($Pr = 0.025$) systems) is upflow (downflow) under depressions for a predominately surface tension (buoyancy driven) driven flow which is accord with observations (see Figs. 6 and 7).

In many of the cases considered herein, except the purely buoyancy driven cases, no definite conclusions could be reached concerning the stability of the system if the seventh disturbance was included. The difficulty arises because of the singularity in the C_h vs h curves which suggests a more refined analysis (possibly including sideband interactions in wavenumber) is necessary and in many cases the occurrence of no stabilizing terms in the amplitude equation associated with the secondary disturbance. The latter occurs due to the signs of the coefficients in its amplitude equation; however, it is noteworthy that in all cases in the buoyancy limit stabilizing terms appeared in accord with the results of Segel [3] and Davis [28]. The secondary stability of most cases investigated here remains an open question both theoretically (modulo this model) and experimentally since either experiments are lacking or do not clearly establish the existence of such stable, stationary flows.

The observations of a flow with hexagonal planform by Bénard [30] and Koschmieder [4] were made using highly viscous ($\mu \simeq 0.1$ Pa s) and thin (4 mm) fluid layers. Estimating the physical parameters for these systems leads to $Cr \sim 10^{-2}$, Pr

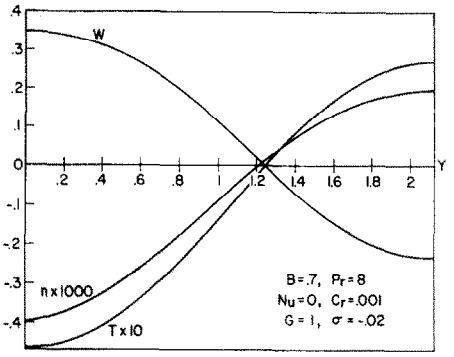

FIG. 6. Typical horizontal variation of vertical velocity, temperature and surface deflection across center of hexagonal cell. Primarily surface tension driven case.

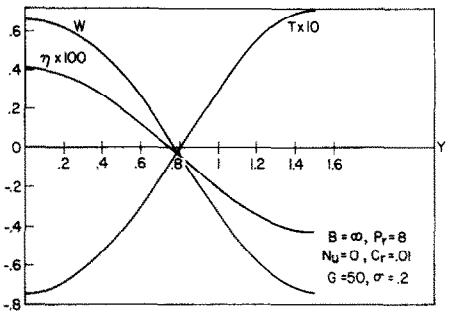

FIG. 7. Typical horizontal variation of vertical velocity, temperature and surface deflection across center of hexagonal cell. Buoyancy driven case.

~ 10000, $B \sim 0.1$ and $G \sim 1$. For this case the theory predicts a stable flow of hexagonal planform with upflow under depressions which can commence at slightly subcritical Marangoni numbers, and hence agrees with observations. (In this case the wave number, α, was set equal to 2.0 since no critical value is predicted by linear stability theory.)

CONVECTIVE STATE PROFILES AND HEAT TRANSFER

Once the appropriate equilibrium amplitudes are calculated the corresponding velocity, temperature or deflection profiles to second order are easily computed. The general form of the expression which encompasses the hexagonal and roll states is

$$
\begin{aligned}
F(\mathbf{x}) = F_1 &\left[B_{1e} \cos \frac{(3)^{1/2}\alpha}{2} x \cos \frac{\alpha y}{2} + B_{6e} \cos \alpha y \right] \\
&+ F_{20}\left(\frac{B_{1e}^2}{4} + \frac{B_{6e}^2}{2} \right) + F_{21} \left[\frac{B_{1e}^2}{4} \cos \alpha y \right. \\
&\left. + B_{1e} B_{6e} \cos \frac{(3)^{1/2}\alpha}{2} x \cos \frac{\alpha y}{z} \right] \\
&+ F_{23} \left[B_{1e} B_{6e} \cos \frac{(3)^{1/2}\alpha}{2} x \cos \frac{3\alpha y}{2} \right. \\
&\left. + \frac{B_{1e}^2}{4} \cos (3)^{1/2} \alpha x \right] \\
&+ F_{24} \left[\frac{B_{1e}^2}{4} \cos (3)^{1/2} \alpha x \cos \alpha y + \frac{B_{6e}^2}{2} \cos 2\alpha y \right], \quad (54)
\end{aligned}
$$

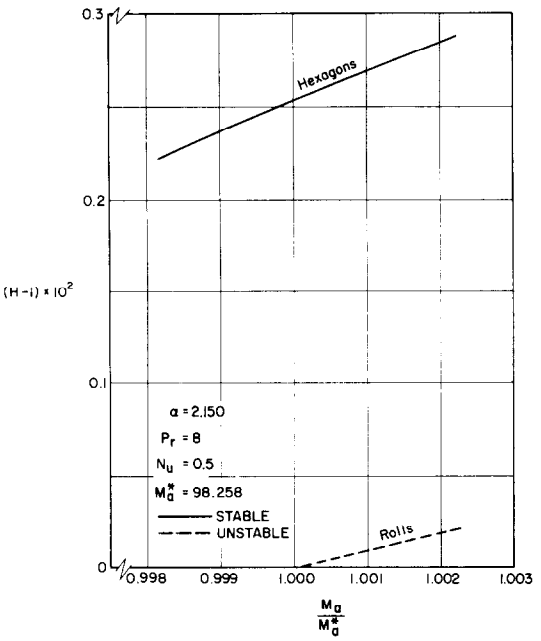

FIG. 8. Dimensionless heat flux.

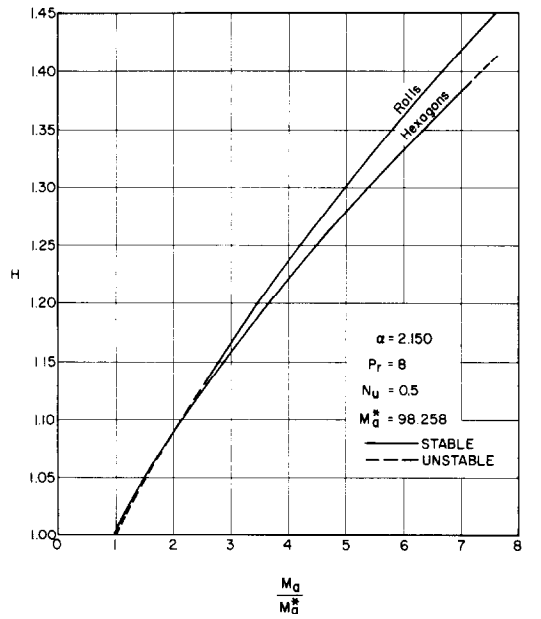

FIG. 9. Dimensionless heat flux.

where F_1, F_{20}, F_{21}, F_{23} and F_{24} are known functions of z. Figures 6 and 7 display a typical set of profiles for a predominately surface tension driven flow and buoyancy driven flow, respectively. Notice that in the predominately surface tension driven flow that there is upflow under depressions and vice versa for the buoyancy driven flow—a feature which agrees with experimental observation.

The maximum absolute magnitude of the deflection in these cases is approximately 0.4% of the layer depth which is consistent with the second order theory presented here.

In order to characterize the cell-mean heat transfer due to each of the ensuing convective flow patterns, it is convenient to form the ratio of the total cell-mean heat flux to that mean flux due to conduction alone, H,-taken at the free surface ($z = 1+\eta$). For convenience this may be taken at the surface $z = 0$, since the sides of the cell correspond to insulated walls. Then, H for hexagons and rolls becomes

$$H_r = 1 + \bar{T}'_{20}|_{z=0}\frac{B_{6e}^2}{2},$$

$$H_h = 1 + \bar{T}'_{20}|_{z=0}\frac{3B_{6e}^2}{2},$$

where an overbar designates a horizontal average. Figures 8 and 9 display this dimensionless heat flux for a typical case driven solely by a gradient in interfacial tension. Note that there is a large region where the roll state transfers more thermal energy than the hexagonal state but is unstable. This result if consistent with the variable property buoyancy driven flows considered by Segel [3] and illustrates an additional case which violates the occasionally invoked principle that the realizable cellular state is that one which maximizes the thermal energy transport. While the validity of the theory is certainly questionable at more than slightly supercritical states, Fig. 8 is included to illustrate that the theory suggests the destabilization of hexagonal cellular flows at supercritical states. It is noteworthy that the great enhancement of the stability of hexagonal flow states (compared to its buoyancy driven counterpart) evident in Fig. 9 is a consequence of the drive mechanism, as previously noted by Scanlon and Segel [16]. As buoyancy effects are increased, the enhancement as well as the region of possible subcritical instability decrease.

DISCUSSION

The convective states with hexagonal, or roll, horizontal planform predicted herein are characteristic of the type of motion sometimes observed experimentally. In these cases the behavior displayed in Fig. 8 as well as the possibility of a subcritical instability are qualitatively correct in general and quantitatively correct for the chosen case. However, the question of the stability of many of the finite amplitude convective states generated during the course of this study to arbitrary disturbances of the same wave number remains unanswered.

REFERENCES

1. M. G. Velardé, Personal communication.
2. S. Chandrasekhar, *Hydrodynamic and Hydromagnetic Stability*. Clarendon Press, Oxford (1961).
3. L. A. Segel, *Non-equil Thermodynamics, Variational Techniques and Stability*, 165. Univ. Chicago Press (1966).
4. E. L. Koschmieder, Bénard convection, *Adv. Chem. Phys.* **26**, 177–212 (1973).
5. R. H. Rogers, Convection, *Rep. Prog. Phys.* **39**, 1–63 (1976).
6. J. R. A. Pearson, On convection cells induced by surface tension, *J. Fluid Mech.* **4**, 489–500 (1958).

7. L. E. Scriven and C. V. Sternling, On cellular convection driven by surface tension gradients: Effects of mean surface curvature and surface viscosity, *J. Fluid Mech.* **19**, 321–340 (1964).
8. K. A. Smith, On convective instability induced by surface tension gradients, *J. Fluid Mech.* **24**, 401–414 (1966).
9. J. C. Berg and A. Acrivos, The Effect of surface active-agents on convection cells induced by surface tension, *Chem. Engng Sci.* **20**, 737–746 (1965).
10. J. C. Berg, Evaporative convection in horizontal fluid layers, Ph.D. Thesis, Univ. California, Berkeley (1964).
11. D. A. Nield, Surface tension and buoyancy effects in cellular convection, *J. Fluid Mech.* **19**, 341–352 (1964).
12. D. A. Nield, Streamlines in Benard convection cells induced by surface tension and buoyancy, *Appl. Math. Phys.* **17**, 226 (1966).
13. P. G. Grodzka and T. C. Bannister, Apollo 17 heat flow and convection experiments, NASA TMX-64772 (1973).
14. E. Speigel and G. Veronis, On the Boussinesq approximation for a compressible fluid, *Astrophys. Jl* **131**, 442–447 (1960).
15. J. Mihaljan, A rigorous exposition of the Boussinesq approximations applicable to a thin layer of fluid, *Astrophys. J.* **136**, 1126–1133 (1962).
16. J. W. Scanlon and L. A. Segel, Finite amplitude cellular convection induced by surface tension, *J. Fluid Mech.* **30**, 149–162 (1967).
17. J. Kraska, Finite amplitude cellular flows in a horizontal fluid layer with a full surface, Ph.D. Thesis, Univ. Illinois (1969).
18. J. T. Stuart, On the non-linear mechanics of hydrodynamic stability, *J. Fluid Mech.* **4**, 1–21 (1958).
19. J. Watson, On the non-linear mechanics of wave disturbances in stable and unstable parallel flows II, *J. Fluid Mech.* **9**, 371–389 (1960).
20. L. A. Segel and J. T. Stuart, On the question of the preferred mode in cellular thermal convection *J. Fluid Mech.* **13**, 289–306 (1962).
21. R. Sani, On finite amplitude roll cell disturbances in a fluid layer subject to heat and mass transfer, *A.I.Ch.E. Jl* **11**, 971–980 (1965).
22. A. Vidal and A. Acrivos, Nature of the neutral state in surface tension driven convection, *Physics Fluids* **9**, 615–616 (1966).
23. V. V. Struminskii, In reference to a nonlinear theory of aerodynamic stability, *Akad. Nauk. SSSR Dokl.* **151**, 1046 (1963).
24. J. T. Stuart, On the cellular patterns in thermal convection, *J. Fluid Mech.* **18**, 481–498 (1964).
25. L. A. Segel, The non-linear interaction of a finite number of disturbances to a layer of fluid heated from below, *J. Fluid Mech.* **21**, 359–384 (1965).
26. D. D. Joseph and C. C. Shir, Subcritical convective instability. I. Fluid layers, *J. Fluid Mech.* **26**, 753–768 (1966).
27. E. Palm and H. Øiann, Contribution to the theory of cellular thermal convection, *J. Fluid Mech.* **19**, 353–365 (1964).
28. S. H. Davis, Buoyancy-surface tension instability by the method of energy, *J. Fluid Mech.* **39**, 347–359 (1969).
29. S. H. Davis and L. A. Segel, Effects of surface curvature and property variation on cellular convection, *Physics Fluids* **11**, 470–477 (1968).
30. H. Bénard, Les tourbillons cellulaires dans une nappe liquide transportant de la chaleur par convection en regime permanent, *Ann. Chem. Phys.* **23**, 62–144 (1901).

CONVECTION DE BÉNARD–RAYLEIGH A AMPLITUDE FINIE

Résumé—On développe une analyse non-linéaire de la convection cellulaire avec force d'Archimède et force de tension de surface dans une couche fluide de profondeur finie et chauffée par le bas. On étudie la structure des cellules hexagonales supercritiques et la configuration de l'écoulement de recirculation ainsi que le flux thermique associé. On décrit une analyse de stabilité d'états possibles d'écoulement.

BÉNARD–RAYLEIGH-KONVEKTION MIT ENDLICHER AMPLITUDE

Zusammenfassung—Eine nichtlineare Analyse der durch Auftrieb und Oberflächenspannungskräfte bewirkten zellularen Konvektion in einer von unten beheizten Fluid-Schicht endlicher Tiefe wird beschrieben. Die Struktur des Strömungsbildes von leicht überkritischen hexagonalen Zellen und von Rollzellen, sowie ihre zugehörigen Wärmeströme werden untersucht. Eine Stabilitätsanalyse der möglichen Strömungszustände wird beschrieben.

КОНВЕКЦИЯ БЕНАРА-РЕЛЕЯ КОНЕЧНОЙ АМПЛИТУДЫ

Аннотация — Описан нелинейный анализ ячеистой конвекции, вызываемой подъёмными силами и силами поверхностного натяжения в нагреваемом снизу слое жидкости конечной толщины. Исследуется структура слабо надкритических шестигранных и валиковых форм течения и характерная для них величина теплового потока. Дан анализ устойчивости возможных конвективных течений.